Published in final edited form as:

Nat Chem Biol. 2019 June ; 15(6): 575–582. doi:10.1038/s41589-019-0293-7.

Structural and mechanistic basis of the mammalian Nudt12 RNA deNADding

Ewa Grudzien-Nogalska[1,3], **Yixuan Wu**[2,3], **Xinfu Jiao**[1], **Huijuan Cui**[1], **Maria K. Mateyak**[1], **Ronald P. Hart**[1], **Liang Tong**[2,*], and **Megerditch Kiledjian**[1,*]

[1]Department Cell Biology and Neuroscience, Rutgers University, Piscataway, NJ 08854

[2]Department Biological Sciences, Columbia University, New York, NY 10027

[3]These authors contributed equally to this work.

Abstract

We recently demonstrated mammalian cells harbor NAD-capped mRNAs that are hydrolyzed by the DXO deNADding enzyme. Here we report the Nudix protein Nudt12 is a second mammalian deNADding enzyme structurally and mechanistically distinct from DXO and targeting different RNAs. Crystal structure of mouse Nudt12 in complex with the deNADding product AMP and three Mg^{2+} ions at 1.6 Å resolution provides exquisite insights into the molecular basis of the deNADding activity within the NAD pyrophosphate. Disruption of the *Nudt12* gene stabilizes transfected NAD-capped RNA in cells and its endogenous NAD-capped mRNA targets are enriched in those encoding proteins involved in cellular energetics. Furthermore, exposure of cells to nutrient or environmental stress manifests changes in NAD-capped RNA levels that are selectively responsive to Nudt12 or DXO respectively, indicating an association of deNADding to cellular metabolism.

The redox cofactor nicotinamide adenine dinucleotide (NAD) was recently reported to be covalently linked to the 5’ end of bacterial RNA[1] primarily on a subset of small regulatory RNAs in a cap-like manner[2]. Addition of the NAD cap to RNAs appears to occur during transcription initiation[3]. The transcriptional incorporation of NAD at the 5’ end is supported by *in vitro* incorporation of NAD as a “non-canonical initiating nucleotide” (NCIN) by bacterial RNA polymerase that can integrate NAD as the first transcribed nucleotide in place of ATP[3–5]. More recently, NAD-capped RNAs were also confirmed in eukaryotes with their identification in *Saccharomyces cerevisiae*[6] and mammalian cells[7]. These findings demonstrate the broad distribution of NAD caps in diverse organisms.

*Correspondence should be addressed to: Megerditch Kiledjian, Phone: (848) 445-0796, kiledjian@biology.rutgers.edu, Liang Tong, Phone: (212) 854-5203, ltong@columbia.edu.

AUTHOR CONTRIBUTIONS

M.K., E.G.N., and L.T. designed the experiments. E.G.N. carried out all experiments unless otherwise indicated. X.J. and H.C. created N12 and N12:DXO CRISPR knockout cell lines. X.J. carried out the initial NAD captureSeq and the assays in Fig. 2. Y.W. and L.T. carried out the structural analysis and interpretations. M.K.M. carried out experiments in Fig S4. R.P.H. carried out all bioinformatics analyses. E.G.N. M.K., L.T., Y.W. and R.P.H. wrote the manuscript.

COMPETING INTERESTS

The authors declare no competing interests.

The bacterial Nudix (nucleoside diphosphate linked to another moiety X) hydrolase NudC, initially described as an NAD/H pyrophosphohydrolase[8], can remove the NAD cap by hydrolyzing the diphosphate linkage to produce nicotinamide mononucleotide (NMN) and 5′ -monophosphate RNA[2]. Bacterial strains lacking NudC exhibit an increase in steady state levels of NAD-capped RNAs, interpreted to function as a stability element in bacteria[2, 3] implicating NudC as a deNADding enzyme that removes the protective NAD cap to promote decay. The NAD cap has been reported to protect RNA from 5′ end degradation by the bacterial RppH Nudix protein and RNaseE nucleases *in vitro*[2]. RppH contributes to the generation of monophosphorylated 5′ end transcripts[9] that can further be subjected to RNaseE directed decay[10].

The mammalian Nudix protein Nudt12 is a close homolog of bacterial NudC[11, 12]. It was identified as an NAD/H diphosphatase with a substrate preference for the reduced nicotinamide dinucleotide[13]. Although Nudt12 was initially shown to localize to peroxisomes when fused to a C-terminal green fluorescent protein[13], immunocytochemistry reveals it is also cytoplasmic in at least kidney cells[14] indicating a cytoplasmic function.

The mammalian non-canonical decapping enzyme, DXO[15] possesses deNADding activity by removing the entire NAD moiety from the 5' end of an NAD-capped RNA in cells[7]. Importantly, in contrast to the canonical N7 methylguanosine (m^7G) cap, the NAD cap promotes, rather than prevents, RNA decay in mammalian cells[7]. Interestingly, removal of DXO from mammalian cells allowed detection of NAD-capped intronic small nucleolar RNAs (snoRNAs), suggesting that NAD caps can also be added to 5′ processed termini, in addition to transcriptional incorporation at the 5′ end, implying the existence of an NAD capping mechanism[7, 16].

In this report, we provide several lines of evidence demonstrating that, in addition to DXO, Nudt12 is a deNADding enzyme that targets RNAs distinct from those subjected to DXO deNADding. We further demonstrate that both enzymes are functional in cells and their removal from cells significantly increases the level of NAD-capped RNA. Moreover, NAD capping can be altered by cellular exposure to stress indicating NAD cap levels can be dynamic and vary with cellular metabolic load.

RESULTS

Mammalian Nudt12 deNADs NAD-capped RNA *in vitro*

Eukaryotic cells possess multiple decapping enzymes which function on distinct mRNA subsets[17]. We reasoned that, analogous to decapping proteins, the recently described DXO/Rai1 family of deNADding enzymes[7, 18] may also be just one of multiple deNADding enzymes that each regulate a subset of RNAs. Two Nudix hydrolase proteins that can hydrolyze free NAD, Nudt12 and Nudt13[13, 19] were initially pursued.

To assess the potential deNADding activity of mouse Nudt12 and Nudt13, both recombinant proteins were incubated either with ^{32}P labeled NAD (NRpp*A; asterisk denotes ^{32}P label and NR denotes nicotinamide ribose, Fig. 1a) or *in vitro* transcribed ^{32}P labeled RNA capped with NAD (NRpp*A-RNA, Fig. 1b). As expected [13, 19], both proteins can hydrolyze

free NAD into nicotinamide monophosphate (NMN; NRp) and adenosine monophosphate (p*A), which can be detected by thin-layer chromatography (TLC) (Fig. 1a). Since NAD-capped RNA deNADding by Nudt12 or Nudt13 is expected to proceed through cleavage within the diphosphate of NRpp*A-RNA, the released unlabeled nicotinamide mononucleotide (NRp) would not be detected by TLC and the labeled p*A-RNA would remain at the origin. Therefore, the reaction products were further treated with nuclease P1, which cleaves all phosphodiester bonds within an RNA and releases the terminal labeled p*A (Fig. 1b). Interestingly, Nudt12 but not Nudt13 possessed NAD cap deNADding activity *in vitro* under the conditions and protein concentrations used (Fig. 1b), suggesting not all NAD hydrolyzing enzymes contain comparable RNA deNADding activity. Consistent with this premise, enhancer of mRNA decapping 3 (Edc3) protein, which is an NAD(H)-binding protein with potential hydrolytic activity on free NAD(H)[23], also failed to exhibit deNADding activity (Supplementary Fig. 1).

The cleavage activity of Nudt12 on NAD-capped RNA substrate is between the diphosphate linkage and similar to the activity observed with NudC[2] yet distinct from that of DXO which removes the intact NAD by cleaving the phosphodiester linkage following the adenosine residue[7] (Supplementary Fig. 2). A comparison of Nudt12 decapping activity on m^7G-capped RNA[20] to that of its deNADding activity revealed a greater level of deNADding relative to decapping (Fig. 1c). Nudt12 deNADding activity was compromised by a catalytically inactive mutant harboring glutamine substitutions for two glutamic acid metal coordination residues (Fig. 1c) that is known to abolish Nudt12 decapping activity[20], demonstrating that the decapping and deNADding activities of Nudt12 utilize the same active site.

Distinct classes of deNADding enzymes

To determine the relative activities of Nudt12 and NudC, their hydrolysis activity on NAD, NAD-capped RNA and m^7G-capped RNA were tested. Under these *in vitro* parameters, both enzymes possessed activity on free NAD, NAD-capped RNA and RNA capped with m^7G (Fig. 2a). The bacterial RppH protein, which was included as a negative control, lacked hydrolytic activity on free NAD as expected (Fig. 2a), but surprisingly contained robust deNADding activity on NAD-capped RNA (Fig. 2a, middle panel). RppH deNADding activity was compromised with a catalytic inactive[20, 21] mutant (Fig. 2b) demonstrating the observed deNADding activity is an intrinsic function of wild type RppH. Collectively, these findings indicate there are at least three classes of deNADding enzymes (Supplementary Table 1). The first is the DXO family of proteins that remove the entire NAD from the 5' end of an RNA[7] (Supplementary Fig. 2). The second is represented by NudC and Nudt12 which cleaves within the pyrophosphate of both NAD and NAD-capped RNA. The third class contains RppH, which does not cleave NAD, but does cleave NAD-capped RNA. The result with RppH is reminiscent of canonical Nudix m^7G decapping enzymes that need to bind the RNA body in order to cleave the cap and contain minimal activity on cap structure alone[20, 22].

Structural insights into Nudt12 deNADding

We determined the crystal structure of the catalytic domain of mouse Nudt12 (residues 126–462) in complex with AMP and 3 Mg^{2+} ions at 1.6 Å resolution (Supplementary Table 2). Nudt12 contains an Ankyrin repeat domain in the N-terminal region, (Supplementary Fig. 3a), which is required for RNA deNADding activity but dispensable for NAD hydrolysis (Supplementary Fig. 3b).

The Nudt12 catalytic domain consists of an N-terminal sub-domain (NTD, residues 126–282), a zinc-binding motif (residues 283–318), and a C-terminal sub-domain (CTD, residues 319–462) (Supplementary Fig. 3a). The conserved Nudix sequence elements are located in the CTD, although the NTD also has the Nudix fold. The catalytic domain forms a dimer with an extensive interface, involving contributions from all three sub-domains (Fig. 3a). The two monomers have essentially the same conformation, with rms distance of 0.46 Å for 303 aligned Cα atoms (Supplementary Fig. 3c). The catalytic domain shares 29% amino acid sequence identity with *E. coli* NudC. While the overall structure of Nudt12 is similar to that of NudC[24], there are also substantial differences between them, especially for the NTD (Supplementary Figure 3c,d). The rms distance in Cα atoms is 2.0 Å for 226 aligned residues between the two proteins.

While we included NAD during crystallization, clear electron density was observed for AMP based on the crystallographic analysis (Fig. 3b), consistent with the catalytic activity of Nudt12 (Supplementary Fig. 3c). AMP is primarily bound to the CTD of one protomer (Fig. 3a). The adenine base is in the *syn* configuration, π-stacked with the side chain of Phe356 on one face and on the other face with that of Tyr318 in the other protomer (Fig. 3b).

The phosphate group of AMP is involved in a large network of interactions with Nudt12, mediated through three Mg^{2+} ions (named Mg1, Mg2 and Mg3) (Fig. 3b). One of the terminal oxygen atoms of the phosphate is a bridging ligand to Mg1 and Mg2, while a second terminal oxygen atom is coordinated to Mg3. Three Glu residues in the Nudix motif are ligands of the Mg^{2+} ions, including Glu370 (bidentate interactions with Mg2 and Mg3), Glu374 (coordinated to Mg1), and Glu415 (bidentate interactions with Mg1 and Mg2). Each Mg^{2+} ion is coordinated octahedrally, and seven water molecules or hydroxide ions complete the coordination spheres, one of which is a bridging ligand between Mg2 and Mg3 (Fig. 3b).

The binding mode of AMP in the current structure has significant differences compared to that of the AMP portion of NAD in the complex with NudC[11, 24] (Fig. 3c). Probably due to the absence of metal ions in the NudC complex, the phosphate group is pushed away from the Glu side chains in the active site, and the distance between the phosphorus atoms in the two structures is 5.4 Å (Fig. 3c). In addition, the adenine base is in the *anti* configuration in one NudC complex structure[24] and both *anti* and *syn* configurations in the other NudC complex structure[11]. On the other hand, the NMN portion of NAD in NudC is located near the AMP in the current structure (Fig. 3d), and a model for the binding mode of NAD to Nudt12 could be built based on this (Fig. 3d).

The model of the NAD complex provides clear molecular insights into the deNADing mechanism. The bridging ligand between Mg2 and Mg3 is located directly beneath the

phosphate group of AMP, with a distance of 3.0 Å to the phosphorus atom (Fig. 3d). It initiates the deNADding reaction by attacking the phosphorus atom. There does not appear to be a general acid from the protein, in Nudt12 or NudC, that can stabilize the oxyanion of the leaving group, and this role might be served by a solvent molecule that becomes bound in the presence of NAD.

Mammalian Nudt12 is a deNADding enzyme in cells

To assess whether Nudt12 contributes to the expression of endogenous NAD-capped RNA in cells, we utilized NAD cap detection and Quantitation (NAD-capQ[18]) approach that detects NAD caps *en masse*. NAD-capQ combines the enzymatic properties of nuclease P1 to release intact NAD from the 5' end of NAD-capped cellular RNA, with a colorimetric NAD quantitation to detect the released NAD (Supplementary Fig. 4a). Following demonstration that both human and mouse Nudt12 possess comparable deNADding activity (Supplementary Fig. 4b), a collection of CRISPR/Cas9n directed individual or double knockout human HEK293T cell lines comprised of a pool of three monoclonal knockout cell lines in the *Nudt12* gene (N12-KO), were generated and used (Fig. 4a). Consistent with Nudt12 functioning as a deNADding enzyme in cells, a 1.5-fold increase in total NAD-capped RNA was detected by NAD-capQ in cells devoid of Nudt12 (N12-KO) compared to the control knockout (Con-KO; Fig. 4b). RNA from a pool of monoclonal cells containing homozygous disruptions in the *DXO* gene DXO-KO[7]); revealed a similar 1.5-fold increase in cellular NAD caps (Fig. 4b). Strikingly, a pool of monoclonal lines harboring homozygous disruption of both the *Nudt12* and *DXO* genes (N12:DXO-KO; Fig. 4a) resulted in 2.7-fold higher levels of NAD caps (Fig. 4b).

To test whether Nudt12 can modulate the stability of NAD-capped RNA in cells, ^{32}P uniformly labeled RNA transcripts containing either NAD or m^{7}G at the 5′-end and 16 consecutive guanosine nucleosides (G_{16}) at the 3′-end to minimize 3′-end decay[25] were transfected into Con-KO or N12-KO cells. RNA was harvested at various times up to 4 h post transfection, resolved and detected. As shown in Fig. 4c, NAD-capped transcripts were more stable in N12-KO than Con-KO cells ($t_{½}$ = 4.1h *versus* 2.2h). In contrast m^{7}G-capped RNA showed similar half-lives in both cell line backgrounds (Fig. 4d) which is consistent with previous studies with a knockout of a single decapping enzyme [15, 26]. We conclude Nudt12 can modulate the stability of NAD-capped RNAs transfected into HEK293T cells. Collectively, these data demonstrate that in addition to DXO[7], Nudt12 is also a deNADding enzyme that can regulate the stability of NAD-capped RNAs in cells and importantly, each deNADding enzyme appear to function on distinct NAD capped RNAs.

Nudt12 preferentially deNADs a subset of mRNAs

To directly determine whether Nudt12 contributes to the expression of specific NAD-capped RNAs in cells we utilized the NAD captureSeq approach which was successfully used to isolate NAD-capped RNAs in bacteria[2], yeast[6] and human[7] cells. Briefly, NAD-capped RNAs are identified by the reaction of the 5' end NAD with ADP ribosylcyclase (ADPRC) to generate an alkyne moiety amendable to click chemistry selective covalent incorporation of biotin and purification of the modified RNA with streptavidin[27]. NAD-captureSeq was carried out with RNAs from HEK293T WT or N12-KO cells. Selecting reference transcripts

with at least a 2-fold increase in N12-KO compared with WT, at least 1 FPKM expression level in N12-KO and ≤5% false discovery rate (FDR) revealed 188 NAD-capped RNAs that were specifically enriched in the N12-KO cells (Supplementary Table 3) suggesting these are targets of Nudt12 deNADding. Importantly, subjecting the RNAs increased in Nudt12 knockout to gene ontology using high stringency (FDR ≤5%, ≥10 transcripts per term) revealed that the proteins they encode are within five major significantly enriched pathways, three biological process (BP) terms and two cellular compartment (CC) terms (Supplementary Fig. 5a). One of these relates to rRNA processing while the remaining are linked with mitochondrial metabolism or translation. Interestingly, while transcripts relating to rRNA processing are enriched, none of the 231 nuclear-encoded ribosomal protein gene transcripts was significantly different in N12-KO. Among the 150 nuclear encoded mitochondrial ribosomal transcripts, 10 are significantly enriched in N12-KO (listed in Supplementary Table 3, beginning with MRPL and MRPS), but none of the mitochondrial encoded transcripts were altered. The mRNAs enriched in N12-KO are associated primarily with respiratory function, suggesting an interaction between cell metabolism and Nud12 deNADding of NAD-capped transcripts.

A subset of the NAD-captureSeq identified RNAs consisting of 5 RNAs implicated in oxidative phosphorylation and 7 randomly selected mRNAs were chosen for further validation (Fig. 5a). We found that 11 out of 12 NAD-capped mRNAs identified from the NAD-captureSeq to be enriched in N12-KO cells were validated by direct quantitative reverse-transcription (qRT)-PCR, while the non-Nudt12 target CKS2 mRNA, was not changed in N12-KO compared to WT cells. Seven of the confirmed genes (COX17, MRPL15, MRPS23, NDUFA4, NDUFB2, NDUFB9, and NDUFS3; highlighted in Supplementary Table 3) were found in the enriched GO terms in Supplementary Fig. 5a. These data further verify Nudt12 as a deNADding enzyme in cells and suggest a role for Nudt12 in nuclear-encoded NAD-capped transcripts encoding proteins with metabolic functions.

Applying similar data analysis to NAD-capped RNAs from DXO-KO cells[7], we found that mRNAs enriched in the absence of Nudt12 were relatively distinct from those enriched when DXO was removed (Supplementary Fig. 5b). Out of 188 unique RefSeq mRNAs enriched in N12-KO, only 13 overlap the 67 RefSeq mRNAs enriched by DXO-KO. Previous analyses identified many more DXO-KO-regulated transcripts from the same samples[7], likely due to the inclusion of contrasting m^7G-capped samples in the earlier analysis, which influenced the statistical evaluation. Interestingly, we found groups of NAD-capped RNA uniquely targeted by each enzyme (Fig. 5b). The hierarchical clustering of all 242 transcripts by replicate sample (Fig. 5b) indicates the distinct patterns of transcripts enriched in Nudt12 (light blue in right colorbar; matching Venn diagram) or DXO (coral in right colorbar). Highlighting the enriched GO terms in the left colorbar, the Nudt12-enriched GO terms are similarly distinct from a major DXO-KO category. Of the 175 genes enriched exclusively in N12-KO, two of the top GO-biological processes are linked to mitochondrial metabolism. In contrast, the most prominent class of NAD-capped RNAs elevated in DXO-KO cells, the small nucleolar RNAs (snoRNAs) and the related small Cajal body RNAs (scaRNAs)[7] (Fig. 5b), were not elevated in NAD captureSeq from cells lacking Nudt12. NAD-capped mRNAs involved in oxidative phosphorylation were specifically enriched in

N12-KO cells (Fig. 5). Collectively, these analyses revealed existence of Nudt12 and DXO responsive NAD-capped RNAs in mammalian cells and a modulation of distinct subset of mRNAs by each deNADding enzyme.

Environmental stress can impact NAD capping

Changes in growth conditions or exposure to environmental stress are often accompanied by changes in cellular NAD metabolism. In human cells, cellular NAD levels increase in response to energy stresses, such as glucose deprivation (GD)[28], fasting[29, 30] and caloric restriction[31], indicating that the nutrient state of a cell influences NAD concentrations. To assess whether physiological changes in cellular NAD can manifest altered NAD cap levels in cells, HEK293T cells were subjected to two distinct environmental stress conditions previously shown to affect cellular NAD metabolism: heat shock (HS)[32] and GD[28]. Cells were treated up to four hours with a 42°C HS or grown in glucose-free medium. Quantitation of NAD caps by NAD-capQ revealed ~2-fold increase in cells exposed to either HS or GD (Fig. 6a). The increase is not restricted to transformed cells. A similar 2-fold increase in NAD cap levels was detected in GD primary human foreskin fibroblast (HFF) cells (Fig. 6a). Importantly, the increases in NAD-capped RNA are not a consequence of increases in cellular NAD levels following stress (Fig. 6b). A 1.4-fold increase in cellular NAD concentration was evident in HEK293T cells following HS, 1.1-fold increase in GD HFF cells and a decrease in HEK293T cells subjected to GD (Fig. 6b).

To assess whether cellular stress contributes to changes in the expression of specific Nudt12 or DXO target NAD-capped RNAs, total NAD-capped RNAs were isolated by NAD-capture analogous to Fig. 5. Six Nudt12 target NAD-capped transcripts validated in Fig. 5a or DXO target NAD-capped mRNAs[7] were randomly chosen and quantified. All six Nudt12 responsive NAD-capped mRNAs tested were preferentially increased after GD but not HS (Fig. 6c) consistent with a role of Nudt12 in modulating mRNAs involved in cellular metabolism. In contrast, four of the six DXO responsive NAD-capped mRNAs tested increased after HS, but not GD (Fig. 6c). These observations demonstrate distinct functions for the two deNADding enzymes following different cellular stresses. Interestingly, the levels of Nudt12 protein remained constant (Supplementary Fig. 6) with HS or GD indicating the increase in NAD-capped Nudt12 target mRNAs were not a function of altered Nudt12 protein concentrations and may involve a regulation of its activity following GD. However, DXO protein levels were found to specifically decrease following HS (Supplementary Fig. 6) consistent with the increase in DXO target NAD-capped mRNA upon HS. Collectively, our data demonstrate NAD-capped mRNA levels are dynamic and can be influenced by cellular exposure to stress. Moreover, NAD-capped mRNA levels are selectively modulated by Nudt12 and DXO following exposure to distinct stress conditions where the contributions of Nudt12 are evident following nutrient stress and DXO following environmental stress.

DISCUSSION

Regulation of mRNA stability is an important post-transcriptional process that impacts eukaryotic gene expression. The presence of NAD caps in organisms ranging from *E. coli* to

humans demonstrates the evolutionary conservation of the noncanonical NAD cap at the 5′ end of RNA transcripts and implies a function in RNA metabolism[16]. In this report, we demonstrate that, similar to the presence of multiple m^{7}G cap decapping enzymes in cells[17], mammalian cells also utilize Nudt12 as a deNADding enzyme in human cells. Nudt12 contains deNADding activity *in vitro* (Fig. 1), in human cells (Fig. 4), and targets a specific group of mRNA for deNADding (Fig. 5). The crystal structure of mouse Nudt12 catalytic domain (residues 126–462) defines the binding mode of the AMP product and three coordinated magnesium ions. The structure also provides detailed insights into the molecular mechanism of the deNADding reaction (Fig. 3) and its distinct hydrolysis at the pyrophosphate linkage in Nudt12 to release NMN from NAD-capped RNA compared to the phosphodiester linkage in DXO that releases an intact NAD [7].

Importantly, Nudt12 is a deNADding enzyme that can promote the decay of NAD-capped RNAs in cells (Fig. 4) and it targets a subset of RNAs that are distinct from that of DXO (Fig. 5). Cells lacking either Nudt12 or DXO protein each contained an ~1.5-fold increase in total NAD-capped cellular RNA and almost 3-fold in the double N12:DXO-KO cells (Fig. 4b) indicating that Nudt12 and DXO target different classes of NAD-capped RNAs for deNADding. Specificity of deNADding enzymes was further supported by identification of responsive target mRNAs. Specific NAD-capped RNAs, including histones and nuclear-encoded mRNAs coding for mitochondrial proteins are relatively enriched in N12-KO cells (Fig. 5b, blue color) while depleted in DXO-KO cells (Fig. 5b, yellow color). Conversely, NAD-capped sno/scaRNAs are highly enriched in DXO-KO cells but not detected in cells lacking Nudt12.

Similar to m^{7}G cap decapping enzymes[17], deNADding enzymes also preferentially target distinct mRNA subsets within different cellular pathways. Intriguingly, 14 (19%) of the mRNAs encoding proteins within the mitochondrial electron transport chain contained NAD-capped versions that were elevated in Nudt12-KO cells ($p=1.79 \times 10^{-16}$; Hypergeometric distribution). These findings support a correlation between Nudt12 deNADding activity and cellular energetics and suggest NAD capping of mRNAs encoding mitochondrial oxidative phosphorylation proteins may be a means of coordinating cellular energy demand with mitochondrial output. However, how the deNADding enzymes differentiate between different RNA substrates and preferentially deNAD specific RNAs remains unknown. Whether Nudt12 and DXO utilize a direct mechanism analogous to Dcp2 binding of a stem loop structure[33, 34] or an indirect mechanism by protein recruitment[35, 36] remains to be determined.

An unexpected outcome of our studies is that the bacterial RppH Nudix protein also possesses deNADding activity, at least *in vitro* (Fig. 2a). The discrepancy with previous report [2] is likely due to different *in vitro* deNADding conditions and different substrate RNAs employed in the two studies, for instance presence of guanosine in +2 position of the RNA we used. The latter feature was recently shown to increase BsRppH deNADding activity compared to RNA variants with the other nucleosides occupying this position[37]. Importantly, RppH, unlike Nudt12 and NudC possess robust deNADding activity on NAD-capped transcripts *in vitro*, but not capable of hydrolyzing free NAD *in vitro* (Fig. 2a), thus defining at least three distinct classes of deNADding enzymes (Supplementary Table 1).

Class I deNADding enzymes consist of the DXO family of proteins which remove an intact NAD from the 5' end of NAD-capped RNAs[7]. Class II consists of proteins that can hydrolyze the pyrophosphate linkage of both free NAD as well as NAD at the 5' end of an RNA and is represented by Nudt12 and NudC. Class III deNADding enzymes only function on NAD-capped RNA but not free NAD with RppH as the founding member.

Another important finding from these studies was the demonstration that environmental stress and nutrient deprivation can both lead to elevation of NAD-capped RNA. NAD levels can fluctuate along with the metabolic state of a cell which prompted us to test whether NAD-capped RNA levels are altered with stress. Intriguingly, although NAD-capped RNA levels increased following two different stress parameters employed, cellular NAD levels did not consistently demonstrate a similar increase (Fig. 6). These findings demonstrate that NAD cap levels can be modulated under stress conditions and this modulation is not necessarily a direct function of cellular NAD levels. Moreover, exposure of cells to nutrient or environmental stress differentially affects Nudt12- and DXO-targeted NAD-capped mRNAs, with Nudt12 functionality apparent under GD and DXO evident under HS. Collectively, alteration of NAD-capped mRNA levels may provide a physiological link between the metabolic state of a cell and its mRNA composition.

ONLINE METHODS

Cell Culture and generation of Nudt12 and N12:DXO CRISPR knockout cell lines

Human embryonic kidney HEK293T cells were obtained from ATCC. Cells were cultured in DMEM medium (Thermo Fisher Scientific) supplemented with 10% fetal bovine serum (Atlanta Biologics), and antibiotics (100 units/ml penicillin and 100 μg/ml of streptomycin) under 5% CO_2 at 37 °C. The three different monoclonal HEK293T cell lines harboring CRISPR-Cas9n double-nick generated distinct homozygous deletions within the *DXO* gene genomic region corresponding to its catalytic site have been reported previously[7]. Nudt12 knockout lines were similarly generated using CRISPR-Cas9n technology with two Nudt12-gRNAs (Supplementary Table 3) designed to target genomic regions of *Nudt12* corresponding to the catalytic site in exon 6. Nudt12:DXO double knockout lines were generated using the Nudt12 cell line and CRISPR-Cas9n technology with two DXO-gRNAs (Supplementary Table 3) designed to target genomic regions of *DXO* corresponding to the catalytic site in exon 4. The genomic modification was screened by PCR and confirmed by sequencing and a Western blot of the three mixed clones for N12-KO or N12:DXOKO is shown in Fig. 4a.

Isolation and identification of NAD-capped RNAs

Total RNA from HEK293T, Con-KO, N12-KO, DXO-KO and N12:DXO-KO cell lines were isolated with TRIzol reagent (Thermo Fisher Scientific). NAD-capped RNAs were isolated using the NAD-RNA capture protocol[2] with minor modification. NAD-capture was carried out with 50 μg total RNA treated with 10 μl 4-pentyn-1-ol (Sigma-Aldrich) and 3 U Adenosine diphosphate-ribosylcyclase (ADPRC) in 100 μl reaction containing 50 mM HEPES, 5 mM $MgCl_2$ (pH 7) and 40 U RNasin® Ribonuclease Inhibitor (Promega) at 37 °C 60 min. The reaction was stopped with phenol/chloroform extraction and RNAs were

precipitated with ethanol in the presence of 2 M (final concentration) ammonium acetate. RNAs with a 5' end NAD were biotinylated by treatment with a copper-catalyzed azide-alkyne cycloaddition (CuAAC) reaction by incubating with 250 μM biotin-PEG3-azide, freshly mixed 1 mM CuSO4, 0.5 mM THPTA, 2 mM Sodium Ascorbate in 100 μl reaction with 50 mM HEPES, 5 mM $MgCl_2$ (pH 7) and 40 U RNasin® Ribonuclease Inhibitor (Promega) at 30 °C for 30 min. RNA was precipitated with ethanol in the presence of 2 mM EDTA and 2 M (final concentration) ammonium acetate. Biotinylated NAD capped RNAs were captured by binding to 20 μl streptavidin magnet beads (Nvigen) at room temperature with gentle rocking for 1 hour in 100 μl binding buffer (1 M NaCl, 10 mM HEPES (pH 7.5) and 5 mM EDTA). The beads were washed three times with wash buffer (8 mM Urea, 50 mM Tris-HCl (pH 7.4), 0.1% IPEGAL) and two washes with nuclease free H_2O. Biotinylated NAD-capped RNAs were eluted by resuspending beads in 100 μl H_2O and heating to 95 °C for 5 min and RNA precipitated with ethanol in the presence of 2 M ammonium acetate. Captured NAD-RNAs were reverse transcribed into cDNA and synthesized into dsDNA with the SMARTer® Universal Low Input RNA Kit for Sequencing (Clontech Laboratories, Inc.) following the manufacturer's protocol. NAD-capture for the qRT-PCR validation studies in Figure 5 were carried out similarly except, 50 ng of *in vitro* transcribed NAD-F.Luc-RNA was included as an internal control for normalization.

In vitro Transcription of NAD-Capped RNAs

RNAs containing different cap structures were synthesized by *in vitro* transcription of plasmid ϕ2.5A- CA2- G16 containing the T7 ϕ2.5 promoter[38] that retained the first adenosine at the transcription start site. All other adenosines within the RNA were replaced by uracils to maintain only one adenosine per RNA and a G-tract of 16 guanosines (G16) was present at the 3′ end[7]. *In vitro* transcription was carried out at 37 °C for 90 min in 50 μl reaction containing 400 ng PCR-generated DNA template, 10 μl 5× transcription buffer, 5 μl DTT (10 mM), 5 μl BSA (10 μg/μl), 5 μl rNTP Mix (5 mM), 2 μl T7 RNA polymerase (Promega) and 1 μl RNasin Ribonuclease Inhibitor (40 U/μl, Promega). To generate NAD-capped RNA, rATP was replaced with ^{32}P-NAD or NAD in the reaction to generate ^{32}P-NAD-cap labeled or unlabeled NAD-capped RNAs, respectively. Transcription in the presence of [α−^{32}P]GTP and 0.5 mM m^7GpppA cap analog (New England BioLabs) minus rATP in the reaction was carried out to produce ^{32}P-uniformly-labeled 5'-end N7-methylated RNA.

RNA in vitro Decapping and deNADding Assays

^{32}P-NAD-cap labeled or ^{32}P-m^7G-capped RNAs were incubated with the indicated amount of recombinant proteins in decapping buffer containing 10 mM Tris-HCl pH 7.5, 100 mM KCl, 2 mM DTT, 2 mM $MgCl_2$ and 2 mM $MnCl_2$ as previously described[39] and incubated at 37 °C for 30 min. Reactions were stopped with 30 mM EDTA. For reactions involving Nuclease P1 treatment, reactions were first extracted with phenol followed by chloroform and 1U of Nuclease P1 (Sigma-Aldrich) was added. The reactions were incubate at 37 °C for 30 min. Decapping products were resolved by PEI-cellulose TLC plates (Sigma-Aldrich) and developed in 0.5 M LiCl or 0.45 M $(NH_4)_2SO_4$ in a TLC chamber at room temperature[40]. deNADding assays in Fig. 4S were similarly carried out except, following termination of the reaction with 30mM EDTA, the RNA were resolved by 15% denaturing

polyacrylamide gel electrophoresis and dried. Reaction products were visualized with a Molecular Dynamics PhosphorImager (Storm860).

RNA *in vivo* decay assay

Indicated cells (8×10^6) were seeded in 100 mm plates one day prior to the experiment. 0.5 μg ^{32}P- uniformly-labeled RNA was mixed with 10 μl P3000 reagent in 250 μl Opti-MEM medium and 15 μl Lipofectamine 3000 was diluted in 250 μl Opti-MEM medium (Thermo Fisher Scientific). The two solutions were mixed and incubated at room temperature for 15 min followed by addition of 3.5 ml Opti-MEM to the RNA-Lipofectamine 3000 complexes and applied to the cell culture plates for 30 min. The cells were washed with Opti-MEM and removed from the dish. Untransfected RNAs were degraded by Micrococcal Nuclease (New England Biolabs) in the presence of 5 mM $CaCl_2$ for 30 min at 37 °C. The transfected cells were equally aliquoted into 60 mm cell culture plates and cultured at 37 °C. Cells were harvested at 0, 1, 2 and 4 hour time points after Micrococcal Nuclease treatment. Total RNA was isolated with TRIzol reagent and equal amounts of total RNA from the different time points were fractionated by 8% polyacrylamide gel with 7 M urea. The remaining ^{32}P-labeled RNA was analyzed by PhosphorImager.

RNA-Seq analysis

RNA was prepared, enriched by NAD-capture, and sequenced as described[7]. Sequences were aligned with human hg19 genome (GRCh37) using the UCSC reference transcript map using Tophat [41] and the resulting binary sequence alignment/map format (BAM) files were sorted, duplicates were removed using Picard (Broad Institute; http://broadinstitute.github.io/picard), and transcripts were quantified using Cuffdiff [41]. Results were exported to the CummeRbund package[41] in R/Bioconductor. Only transcripts with expression levels of FPKM (fragments per kilobase of transcript length per million aligned reads) greater than 1.0 in the knockout condition were considered to be detectable. Sequencing data have been deposited in the Gene Expression Omnibus (GEO) database (accession no. GSE90884 (DXO-KO) and GSE110801 (N12-KO).

Protein Expression, Purification and Crystallization

NudC recombinant protein was kindly provided by Bryce Nickels (Waksman Institute of Microbiology, Rutgers University). Nudt12, Nudt13 and RppH recombinant proteins carrying an N-terminal His-tag were expressed from plasmids pET28a-Nudt12, pET28a-Nudt13 and pET28a-RppH described previously[20].

Residues 126–462 of wild-type mouse Nudt12 were sub-cloned into the pET28a vector (Novagen), and the recombinant protein contained an N-terminal His-tag. This purified wild-type protein did not produce any crystallization hits. The E219A/E220A/E221A triple mutation was introduced using Transfer-PCR method [42]. The mutant protein was expressed in *Escherichia coli* BL21(DE3) Star cells at 20 °C for 18 h. The cells were lysed by sonication in a buffer containing 20 mM Tris (pH 8.0), 250 mM NaCl, and 5% (v/v) glycerol. The lysate was loaded onto an Ni-NTA (Qiagen) column. The eluted protein was treated overnight with thrombin at 4 °C to remove the His-tag and was further purified by gel filtration chromatography (Sephacryl S-300; GE healthcare). The purified protein was

concentrated to 23 mg/ml in a solution containing 20 mM Tris (pH 8.0), 200 mM NaCl, and 5 mM DTT before being flash-frozen in liquid nitrogen and stored at –80 °C.

For crystallization, the above triple mutate protein at 8 mg/ml concentration was incubated with 1.5 mM NAD (Sigma) in a buffer containing 20 mM Tris (pH 8.0), 200 mM NaCl, 5 mM DTT, and 2 mM $MgCl_2$ at 4 °C for 30 min. Crystals were obtained at 20 °C using the sitting-drop vapor-diffusion method. The reservoir solution contained 0.1 M HEPES (pH 7.5) and 24% (w/v) PEG2000MME. The crystals were cryo-protected by the reservoir solution supplemented with 15% (v/v) ethylene glycol and were flash-frozen in liquid nitrogen for data collection at 100K.

Data Collection and Structure Determination

X-ray diffraction data were collected using the Pilatus-6M detector at the Advanced Photon Source (APS) beamline 24-ID-C. The X-ray wavelength was 0.9791 Å. The diffraction images were processed and scaled using the XDS program [43]. The crystal belonged to space group *P*1 with unit cell dimensions of $a = 56.2$ Å, $b = 58.6$ Å, $c = 61.7$ Å. There is a Nudt12 homodimer in the crystallographic asymmetric unit.

The catalytic domain of Nudt12 shares 29% sequence identity with NudC, and a molecular replacement solution could readily be found using the structure of NudC as the search model[24] with the program Phaser[44]. However, the resulting electron density map was not of sufficient quality to rebuild the model. To obtain separate phase information, the CTD of Nudt12 was located using the molecular replacement method. The phase information from this model was used to calculate an anomalous difference electron density map, which clearly revealed the positions of the two zinc atoms (with 11α peak heights), even though the diffraction data were collected far above the zinc absorption edge. Phase information from anomalous scattering was combined with that from the model, and the CTD could be rebuilt automatically using the resulting map with PHENIX[45]. Several β-strands in the NTD and segments near the zinc could be built manually with the program Coot[46] and were included in the subsequent structure refinement with PHENIX, which led to an improved $2F_o–F_c$ map. The entire structure was obtained after several rounds of manual model building followed by refinement. In the final model, 98.7% of the residues are in the favored region of the Ramachandran plot, and 0.16% (1 residue) is located just outside of the allowed region. The crystallographic information is summarized in Supplementary Table 1.

RNA isolation, reverse transcription, and real-time qRT-PCR

Total cellular RNA was harvested with TRIzol Reagent (Thermo Fisher Scientific) and treated with DNase (Promega) according to the manufacturers' protocols. Reverse transcription was performed on 2 μg of RNA in 20-μl reaction mixtures with M-MLV reverse transcriptase, random hexamers, and oligo(dT) (Promega) according to the manufacturer's instructions. qRT-PCR was performed with the primers listed in a Supplementary Table 4. qRT-PCR was carried out on Rotor-Gene 3000 (Corbett Research) with iTaq SYBR Green Supermix (Bio-Rad Laboratories). Relative mRNA levels were normalized to 18S rRNA and calculated as described in User Bulletin No. 2 for the ABI Prism 7700 Sequence Detection System.

NAD-cap detection and Quantitation

HEK293T cells (6×10^6) were seeded in 100 mm plates a day before the experiment and cells were harvested for protein or RNA extraction at ~ 80% confluency. NAD-capQ was carried out as described[18]. To measure NAD-cap amounts on RNA, total cellular RNA was extracted with TRIzol Reagent according to the manufacture's protocol (Thermo Fisher Scientific). To maximize removal of potential residual free NAD copurifying with the RNA, isolated RNA was dissolved in 10 mM Tris-HCl (pH 7.5) containing 2 M urea. Samples were incubated 2 min at 65 °C and immediately precipitated with isopropanol in the presence of 2 M (final concentration) ammonium acetate. Fifty micrograms of total RNA was subjected to NAD-Cap Detection and Quantitation (NAD-capQ) assay as described[18]. Briefly, total RNA was digested with 1 U of Nuclease P1 (Sigma-Aldrich) in 20 μl of 10 mM Tris (pH 7.0), 20 μM $ZnCl_2$ at 37 °C for 20 min to release 5' end NAD. The control samples were prepared by incubating 50 μg of RNA treated with the same reaction condition including 10% glycerol used to dissolve the enzyme, but lacked Nuclease P1. After the reaction, 30 μl of NAD/NADH Extraction Buffer (NAD/NADH Quantitation Kit, Sigma-Aldrich) was added to each sample. In the second step, 50 μl samples were used to perform the colorimetric assay according to the manufacture's protocol (NAD/NADH Quantitation Kit, Sigma-Aldrich).

Cellular total NAD quantitation

HEK293T cells (6×10^6) were seeded in 100 mm plates a day before the experiment. Cells were ~ 80% confluent at the time of protein extraction. To measure cellular total NAD levels, 1/5 of the cells were lysed in 400 μl of NAD/NADH Extraction Buffer (NAD/NADH Quantitation Kit, Sigma-Aldrich) and total protein was extracted by two freeze/thaw cycles (20 min on dry –ice, then 15 min at RT). Cell lysates were centrifuged at 13,000g at 4°C for 10 min and supernatant was taken to measure protein concentration. 10 μg of total proteins were used to detect cellular NAD according to the manufacture's protocol (NAD/NADH Quantitation Kit, Sigma).

Western blot analysis

Cells were lysed in phosphate-buffered saline containing 0.5% IGEPAL CA-630 (Sigma-Aldrich), protease inhibitors (Roche Applied Science) and sonicated. Equal protein amounts of the different samples were separated by Bolt 4–12% Bis-Tris Plus Gel (Thermo Fisher Scientific) and transferred to nitrocellulose membranes (Bio-Rad). The blots were incubated with primary antibodies in phosphate-buffered saline buffer supplemented with 5% BSA (Sigma-Aldrich), then with secondary antibodies conjugated to horseradish peroxidase. Proteins were detected using the ECL western blotting substrate (Thermo Fisher Scientific). The following antibodies were used in this study: rabbit polyclonal anti-DXO (Dom3Z) (Proteintech, cat# 11015–2-AP); rabbit polyclonal anti-Nudt12 (Abcam, cat# ab197310); mouse monoclonal anti-GAPDH (Sigma-Aldrich, cat# G8795) and mouse monoclonal anti-β-Tubulin (Sigma-Aldrich, cat# T8328).

QUANTIFICATION AND STATISTICAL ANALYSIS

mRNA half-lives of reporter mRNAs were obtained by constructing linear models of the ln[remaining RNA] as a function of time, and then the half-life calculated as the ln[2]/slope[47]. All data are presented ± the 95% confidence interval and p values were calculated from the linear model using R[48,49].

Following alignment with genome sequences, sequencing reads were assembled with the UCSC hg19 reference transcript map using Cufflinks, allowing a direct comparison of expression levels by Cuffdiff. Results were exported to the CummeRbund package[41] in R/Bioconductor[48,49]. Only transcripts with expression levels of FPKM (fragments per kilobase of transcript length per million aligned reads) greater than 1.0 in at least one condition were considered to be expressed.

DATA AVAILABILITY

The data that support the findings of this study are available from the corresponding author upon reasonable request. Sequencing data have been deposited in the Gene Expression Omnibus (GEO) database (accession no. GSE90884 (DXO-KO) and GSE110801 (N12-KO). The atomic coordinates have been deposited at the Protein Data Bank (PDB entry 6O3P).

Supplementary Material

Refer to Web version on PubMed Central for supplementary material.

ACKNOWLEDGEMENTS

This work was supported by National Institutes of Health (NIH) grant GM118093 and S10OD012018 (L.T.) and GM126488 (M.K.). We thank B.E. Nickels for helpful discussions and providing recombinant NudC. We thank K. Perry and R. Rajashankar for access to the NE-CAT 24-C beamline at the Advanced Photon Source. This work is based upon research conducted at the Northeastern Collaborative Access Team beamlines, funded by the NIH (P41 GM103403). The Pilatus 6M detector on 24-ID-C beam line is funded by a NIH-ORIP HEI grant (S10 RR029205). This research used resources of the Advanced Photon Source, a U.S. Department of Energy (DOE) Office of Science User Facility operated by Argonne National Laboratory under Contract No. DE-AC02–06CH11357. Computational resources were provided by the Office of Advanced Research Computing (OARC) at Rutgers, The State University of New Jersey, under the National Institutes of Health Grant No. S10OD012346.

REFERENCES

1. Chen YG, Kowtoniuk WE, Agarwal I, Shen Y & Liu DR LC/MS analysis of cellular RNA reveals NAD-linked RNA. Nat Chem Biol 5, 879–81 (2009). [PubMed: 19820715]
2. Cahova H, Winz ML, Hofer K, Nubel G & Jaschke A NAD captureSeq indicates NAD as a bacterial cap for a subset of regulatory RNAs. Nature 519, 374–7 (2015). [PubMed: 25533955]
3. Bird JG et al. The mechanism of RNA 5' capping with NAD+, NADH and desphospho-CoA. Nature 535, 444–7 (2016). [PubMed: 27383794]
4. Malygin AG & Shemyakin MF Adenosine, NAD and FAD can initiate template-dependent RNA synthesis catalyzed by Escherichia coli RNA polymerase. FEBS Lett 102, 51–4 (1979). [PubMed: 222618]
5. Julius C & Yuzenkova Y Bacterial RNA polymerase caps RNA with various cofactors and cell wall precursors. Nucleic Acids Res 45, 8282–8290 (2017). [PubMed: 28531287]
6. Walters RW et al. Identification of NAD+ capped mRNAs in Saccharomyces cerevisiae. Proc Natl Acad Sci U S A 114, 480–485 (2017). [PubMed: 28031484]

7. Jiao X et al. 5’ End Nicotinamide Adenine Dinucleotide Cap in Human Cells Promotes RNA Decay through DXO-Mediated deNADding. Cell 168, 1015–1027 e10 (2017). [PubMed: 28283058]
8. Frick DN & Bessman MJ Cloning, purification, and properties of a novel NADH pyrophosphatase. Evidence for a nucleotide pyrophosphatase catalytic domain in MutT-like enzymes. J Biol Chem 270, 1529–34 (1995). [PubMed: 7829480]
9. Luciano DJ, Vasilyev N, Richards J, Serganov A & Belasco JG Importance of a diphosphorylated intermediate for RppH-dependent RNA degradation. RNA Biol, 1–15 (2018).
10. Mackie GA Ribonuclease E is a 5’-end-dependent endonuclease. Nature 395, 720–3 (1998). [PubMed: 9790196]
11. Zhang D et al. Structural basis of prokaryotic NAD-RNA decapping by NudC. Cell Res 26, 1062–6 (2016). [PubMed: 27561816]
12. Srouji JR, Xu A, Park A, Kirsch JF & Brenner SE The evolution of function within the Nudix homology clan. Proteins 85, 775–811 (2017). [PubMed: 27936487]
13. Abdelraheim SR, Spiller DG & McLennan AG Mammalian NADH diphosphatases of the Nudix family: cloning and characterization of the human peroxisomal NUDT12 protein. Biochem J 374, 329–35 (2003). [PubMed: 12790796]
14. Carreras-Puigvert J et al. A comprehensive structural, biochemical and biological profiling of the human NUDIX hydrolase family. Nat Commun 8, 1541 (2017). [PubMed: 29142246]
15. Jiao X, Chang JH, Kilic T, Tong L & Kiledjian M A mammalian pre-mRNA 5’ end capping quality control mechanism and an unexpected link of capping to pre-mRNA processing. Mol Cell 50, 104–15 (2013). [PubMed: 23523372]
16. Kiledjian M Eukaryotic RNA 5’-End NAD(+) Capping and DeNADding. Trends Cell Biol 28, 454–464 (2018). [PubMed: 29544676]
17. Grudzien-Nogalska E & Kiledjian M New insights into decapping enzymes and selective mRNA decay. Wiley Interdiscip Rev RNA 8(2017).
18. Grudzien-Nogalska E, Bird JG, Nickels BE & Kiledjian M “NAD-capQ” detection and quantitation of NAD caps. RNA 24, 1418–1425 (2018). [PubMed: 30045887]
19. Abdelraheim SR, Spiller DG & McLennan AG Mouse Nudt13 is a Mitochondrial Nudix Hydrolase with NAD(P)H Pyrophosphohydrolase Activity. Protein J 36, 425–432 (2017). [PubMed: 28755312]
20. Song MG, Bail S & Kiledjian M Multiple Nudix family proteins possess mRNA decapping activity. RNA 19, 390–9 (2013). [PubMed: 23353937]
21. Mildvan AS et al. Structures and mechanisms of Nudix hydrolases. Arch Biochem Biophys 433, 129–43 (2005). [PubMed: 15581572]
22. Walters RW, Shumilin IA, Yoon JH, Minor W & Parker R Edc3 function in yeast and mammals is modulated by interaction with NAD-related compounds. G3 (Bethesda) 4, 613–22 (2014). [PubMed: 24504254]
23. Piccirillo C, Khanna R & Kiledjian M Functional characterization of the mammalian mRNA decapping enzyme hDcp2. Rna 9, 1138–47 (2003). [PubMed: 12923261]
24. Hofer K et al. Structure and function of the bacterial decapping enzyme NudC. Nat Chem Biol 12, 730–4 (2016). [PubMed: 27428510]
25. Wang Z & Kiledjian M Functional Link between the Mammalian Exosome and mRNA Decapping. Cell 107, 751–762. (2001). [PubMed: 11747811]
26. Song MG, Li Y & Kiledjian M Multiple mRNA decapping enzymes in mammalian cells. Mol Cell 40, 423–32 (2010). [PubMed: 21070968]
27. Winz ML et al. Capture and sequencing of NAD-capped RNA sequences with NAD captureSeq. Nat Protoc 12, 122–149 (2017). [PubMed: 27977022]
28. Fulco M et al. Glucose restriction inhibits skeletal myoblast differentiation by activating SIRT1 through AMPK-mediated regulation of Nampt. Dev Cell 14, 661–73 (2008). [PubMed: 18477450]
29. Canto C et al. AMPK regulates energy expenditure by modulating NAD+ metabolism and SIRT1 activity. Nature 458, 1056–60 (2009). [PubMed: 19262508]
30. Canto C et al. Interdependence of AMPK and SIRT1 for metabolic adaptation to fasting and exercise in skeletal muscle. Cell Metab 11, 213–9 (2010). [PubMed: 20197054]

31. Chen D et al. Tissue-specific regulation of SIRT1 by calorie restriction. Genes Dev 22, 1753–7 (2008). [PubMed: 18550784]
32. Raynes R et al. The SIRT1 modulators AROS and DBC1 regulate HSF1 activity and the heat shock response. PLoS One 8, e54364 (2013). [PubMed: 23349863]
33. Li Y, Ho ES, Gunderson SI & Kiledjian M Mutational analysis of a Dcp2-binding element reveals general enhancement of decapping by 5'-end stem-loop structures. Nucleic Acids Res 37, 2227–37 (2009). [PubMed: 19233875]
34. Li Y, Song MG & Kiledjian M Transcript-specific decapping and regulated stability by the human Dcp2 decapping protein. Mol Cell Biol 28, 939–48 (2008). [PubMed: 18039849]
35. Arribas-Layton M, Wu D, Lykke-Andersen J & Song H Structural and functional control of the eukaryotic mRNA decapping machinery. Biochim Biophys Acta 1829, 580–9 (2013). [PubMed: 23287066]
36. Li Y & Kiledjian M Regulation of mRNA decapping. Wiley Interdiscip Rev RNA 1, 253–65 (2010). [PubMed: 21935889]
37. Frindert J et al. Identification, Biosynthesis, and Decapping of NAD-Capped RNAs in B. subtilis. Cell Rep 24, 1890–1901 e8 (2018). [PubMed: 30110644]
38. Coleman TM, Wang G & Huang F Superior 5' homogeneity of RNA from ATP-initiated transcription under the T7 phi 2.5 promoter. Nucleic Acids Res 32, e14 (2004). [PubMed: 14744982]
39. Jiao X et al. Identification of a quality-control mechanism for mRNA 5'-end capping. Nature 467, 608–11 (2010). [PubMed: 20802481]
40. Liu SW, Jiao X, Welch S & Kiledjian M Analysis of mRNA decapping. Methods Enzymol 448, 3–21 (2008). [PubMed: 19111168]
41. Trapnell C et al. Differential gene and transcript expression analysis of RNA-seq experiments with TopHat and Cufflinks. Nat Protoc 7, 562–78 (2012). [PubMed: 22383036]
42. Erijman A, Dantes A, Bernheim R, Shifman JM & Peleg Y Transfer-PCR (TPCR): a highway for DNA cloning and protein engineering. J Struct Biol 175, 171–7 (2011). [PubMed: 21515384]
43. Kabsch W Integration, scaling, space-group assignment and post-refinement. Acta Crystallogr D Biol Crystallogr 66, 133–44 (2010). [PubMed: 20124693]
44. McCoy AJ et al. Phaser crystallographic software. J Appl Crystallogr 40, 658–674 (2007). [PubMed: 19461840]
45. Adams PD et al. PHENIX: building new software for automated crystallographic structure determination. Acta Crystallogr D Biol Crystallogr 58, 1948–54 (2002). [PubMed: 12393927]
46. Emsley P & Cowtan K Coot: model-building tools for molecular graphics. Acta Crystallogr D Biol Crystallogr 60, 2126–32 (2004). [PubMed: 15572765]
47. Andersen J, VanScoy S, Cheng TF, Gomez D & Reich NC IRF-3-dependent and augmented target genes during viral infection. Genes Immun 9, 168–75 (2008). [PubMed: 18094709]
48. Dudoit S, Gentleman RC & Quackenbush J Open source software for the analysis of microarray data. Biotechniques Suppl, 45–51 (2003). [PubMed: 12664684]
49. Gentleman RC et al. Bioconductor: open software development for computational biology and bioinformatics. Genome Biol 5, R80 (2004). [PubMed: 15461798]

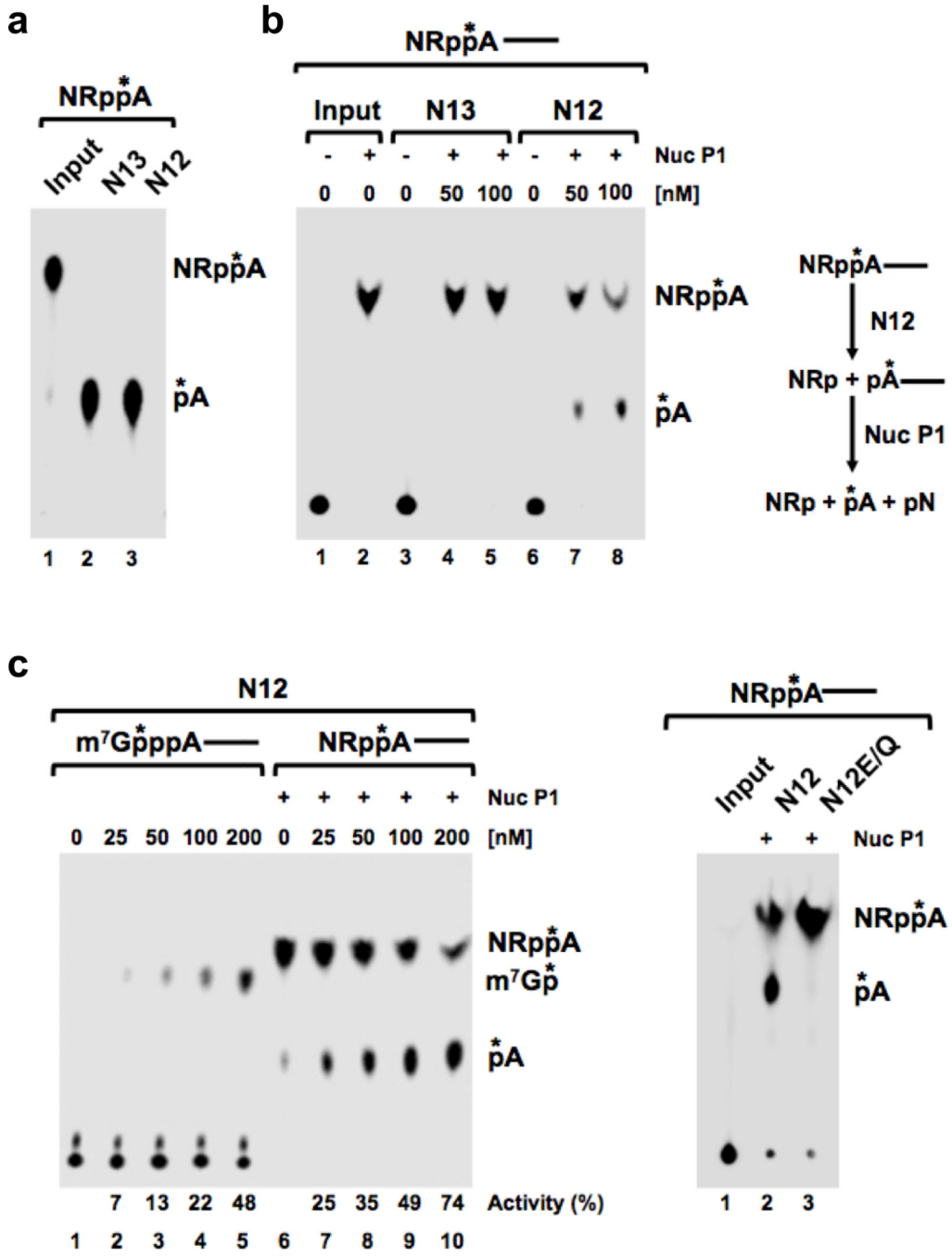

Figure 1. Mammalian Nudt12 possesses robust deNADding activity *in vitro*

(a) Mouse Nudt12 (N12) and Nudt13 (N13) can hydrolysis free NAD. Reaction products of ^{32}P-labeled free NAD (NRpp*A) were resolved by polyethyleneimine (PEI)-cellulose thin-layer chromatography (TLC) developed in 0.5 M LiCl. NR denotes nicotinamide and the asterisk indicates position of the ^{32}P.

(b) Nudt12, but not Nudt13, deNADs NAD-capped RNA. NAD-capped RNA (NRpp*A------) where the line represents RNA and addition of Nuclease P1 to cleave all phosphodiester bonds is denoted by Nuc P1. Reaction products of NAD-capped RNA were

resolved as in panel **a**, and (+) indicates additional treatment with Nuclease P1. A schematic of the NAD-capped RNA substrate and hydrolyzed products is shown. Labeling is as described in **a** above.

(c) In vitro decapping/deNADding assays with mouse Nudt12 protein and indicated ^{32}P-cap-labeled substrates. Catalytically inactive double-mutant Nudt12E373Q/E374Q (N12E/Q) lacks deNADding activity. Labeling is as described in **a** above.

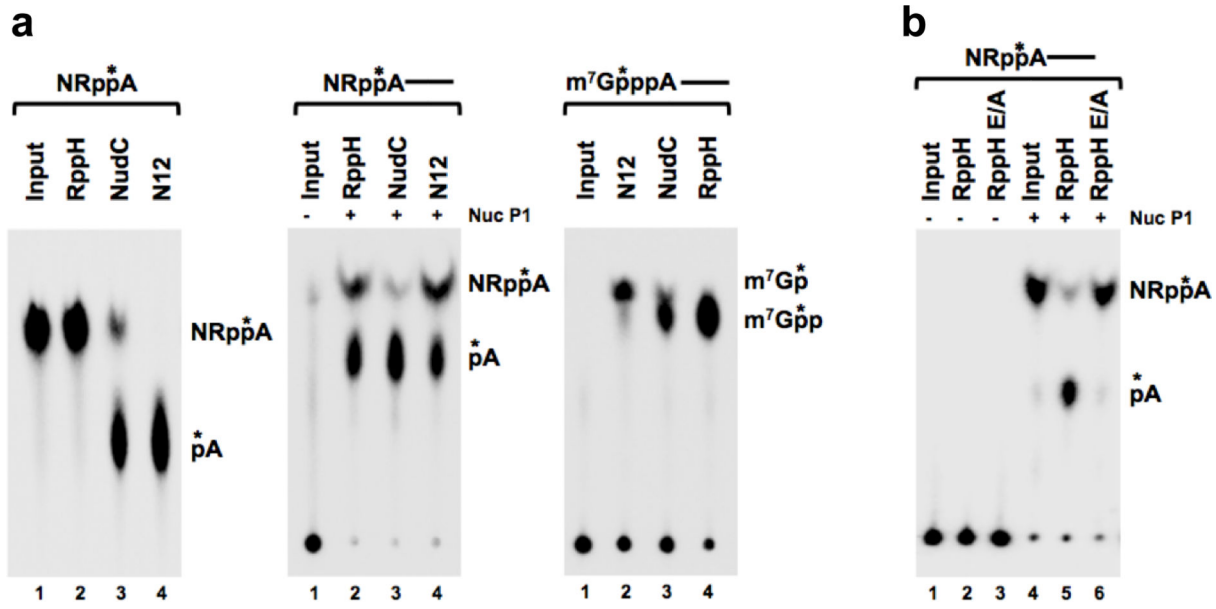

Figure 2. RppH has RNA deNADding activity *in vitro*

(a) *E. coli* RppH is a robust deNADding enzyme. *In vitro* decapping assays were carried out in buffer containing both Mn^{2+} and $Mg^{2+}$with 50 nM RppH, NudC or mouse Nudt12 and ^{32}P-labeled substrates: free NAD (left panel), 30-nt NAD-capped RNA possessing guanosine in +2 position (middle panel) and 30-nt m^7G-capped RNA (right panel). Labeling is as described in the legend to Fig. 1 and TLC was developed in 0.45 M $(NH_4)_2SO_4$.

(b) Catalytically inactive mutant RppHE53A (RppH E/A) lacks deNADding activity. *In vitro* deNADding assays were carried out with 100 nM *E. coli* RppH or RppH E/A proteins and ^{32}P-labeled NAD-capped RNA substrate. TLC was developed in 0.5 M LiCl.

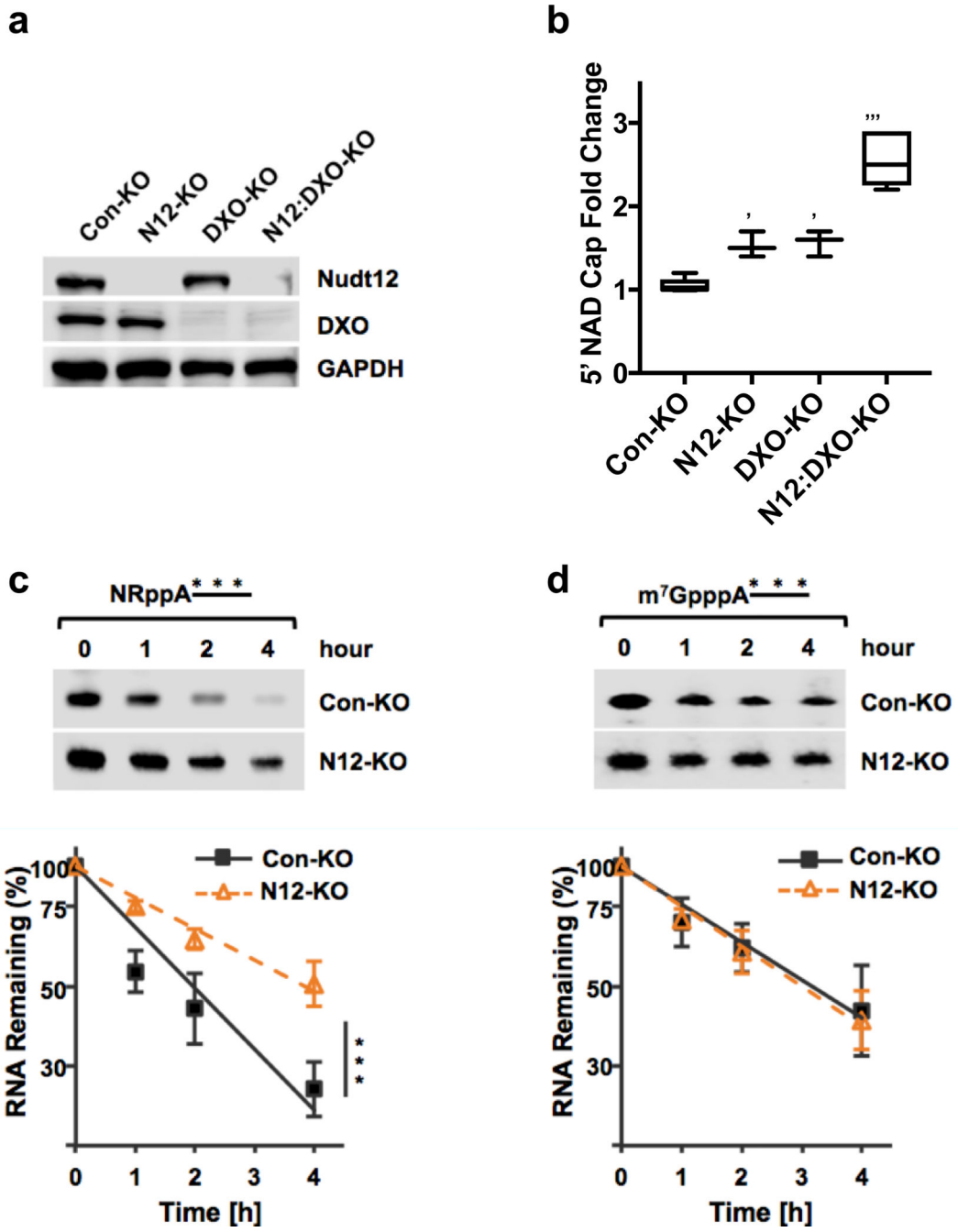

Figure 3. Crystal structure of mouse Nudt12 in complex with AMP and 3 Mg^{2+} ions

(a) Two views of the crystal structure at 1.6 Å resolution of mouse Nudt12 catalytic domain in complex with AMP and 3 Mg^{2+} ions. The two monomers are colored green and cyan, respectively. AMP is shown as stick models in black, Mg^{2+} ions as pink spheres, and Zn as gray spheres. A disulfide bond between residues 177 and 247, formed during crystallization, is indicated as stick models.

(b) Detailed binding mode of AMP and Mg^{2+} ions in Nudt12. The coordination sphere of each metal ion is indicated with the red dashed lines. Water molecules are shown as red

spheres. The omit F_o–F_c electron density at 1.6 Å resolution for AMP, Mg^{2+} ions and their water ligands is shown in wheat color, contoured at 5 σ.

(c) Comparison to the binding mode of NAD in NudC. Overlay of the structure of Nudt12 (in color) in complex with AMP (black) and three Mg^{2+} ions (pink) with that of NudC in complex with NAD (gray, PDB entry 5IW4). The position of the phosphate of AMP is separated by 5.4 Å from the equivalent phosphate of NAD, indicated with the black arrow.

(d) Molecular mechanism of the deNADding reaction. A model of the binding mode of NAD is shown (salmon color). The AMP portion of the model is identical to the crystal structure, and the NMN portion is based on that in the NudC complex. The nucleophilic attack by the bridging ligand of Mg2 and Mg3 on the phosphate is indicated by the black arrow, which initiates the deNADding reaction. The water molecule that is displaced in the NAD complex is indicated with the arrowhead (red).

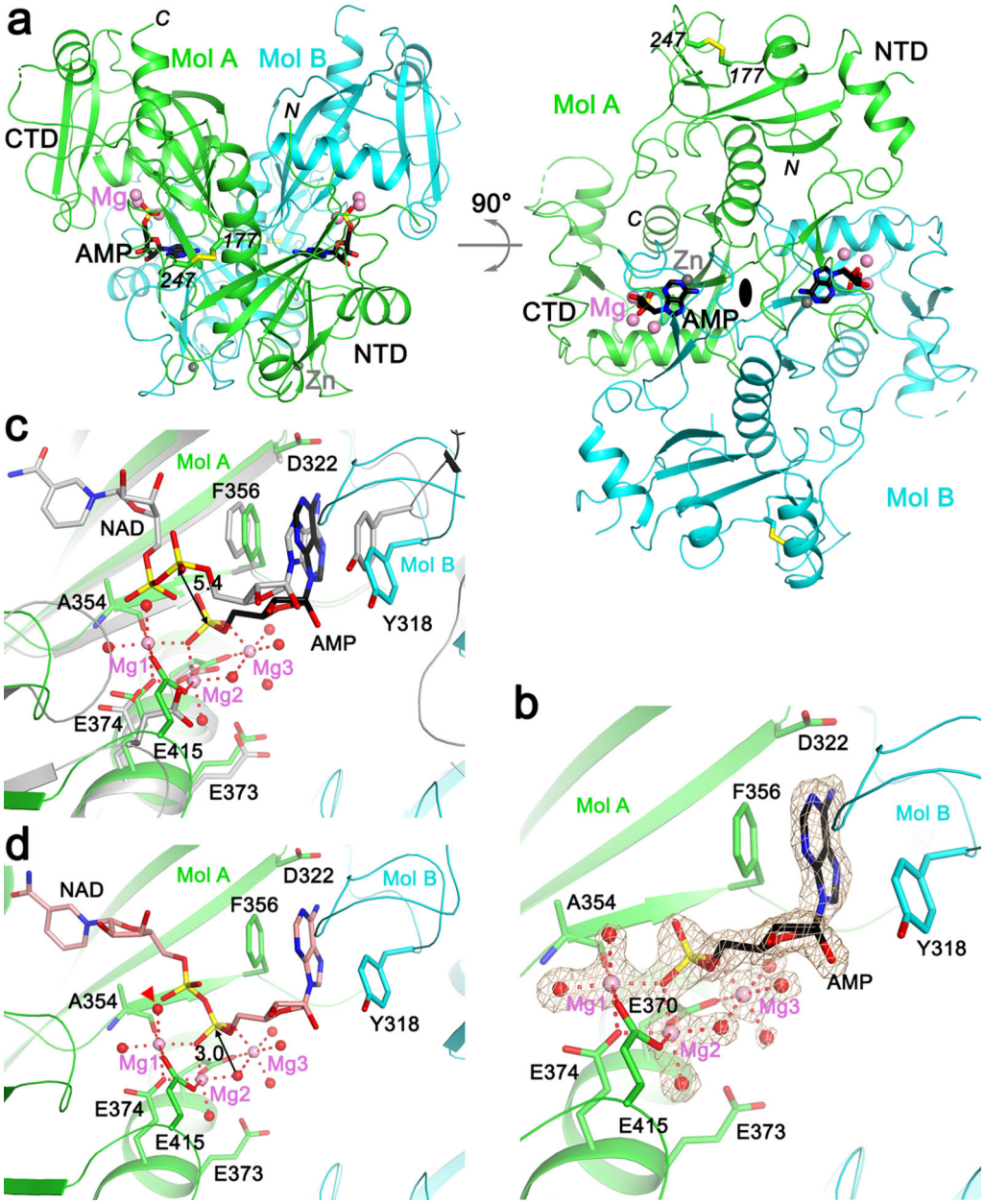

Figure 4. Mammalian Nudt12 is a deNADding enzyme in cells

(a) Western blot analysis of Nudt12 and DXO protein levels in HEK293T control knockout (Con-KO), Nudt12 knockout (N12-KO), DXO knockout (DXO-KO) or double knockout (N12:DXO-KO) cell lines. GAPDH was used as an internal control. See Supplementary Fig 7 for extended Western blot.

(b) Total RNA from the indicated mammalian cells were subjected to NAD-capQ to detect levels of NAD-caps. Data represents the average from at least three independent experiments and is presented in box plots. The boxes indicate standard deviation from the mean, line is the median, and whiskers represent 95% confidence interval. Error bars represent ± SEM. Statistical significance level was calculated by one-way ANOVA ($F=53.34$, $df=7.79$, $p < 0.0001$) with a Dunnett's multiple comparison post hoc test, * $p \leq 0.05$, *** $p \leq 0.001$.

(c) ^{32}P uniformly labeled NAD-capped RNA, or **(d)** m^{7}G-capped RNA were transfected into the indicated cell lines using Lipofectamine 3000. Untransfected RNAs were degraded with micrococcal nuclease (MN), and total RNA was isolated at the times denoted following micrococcal nuclease treatment. Remaining RNA was resolved on 8% denaturing PAGE, exposed to a PhosphorImager, quantitated and plotted. All data are derived from three independent experiments with ±SEM denoted by the error bars. Linear regression was used to fit the time course data to an equation with or without the category labels (Con-KO or N12-KO). Statistical significance level was calculated by comparing these two models with one-way ANOVA ($F=25.303$, $df=26$; $p \leq 0.001$ (***); Con-KO $t_{½}$ = 4.1h, N12-KO $t_{½}$ = 2.2h). See Supplementary Fig 8 for extended RNA gels.

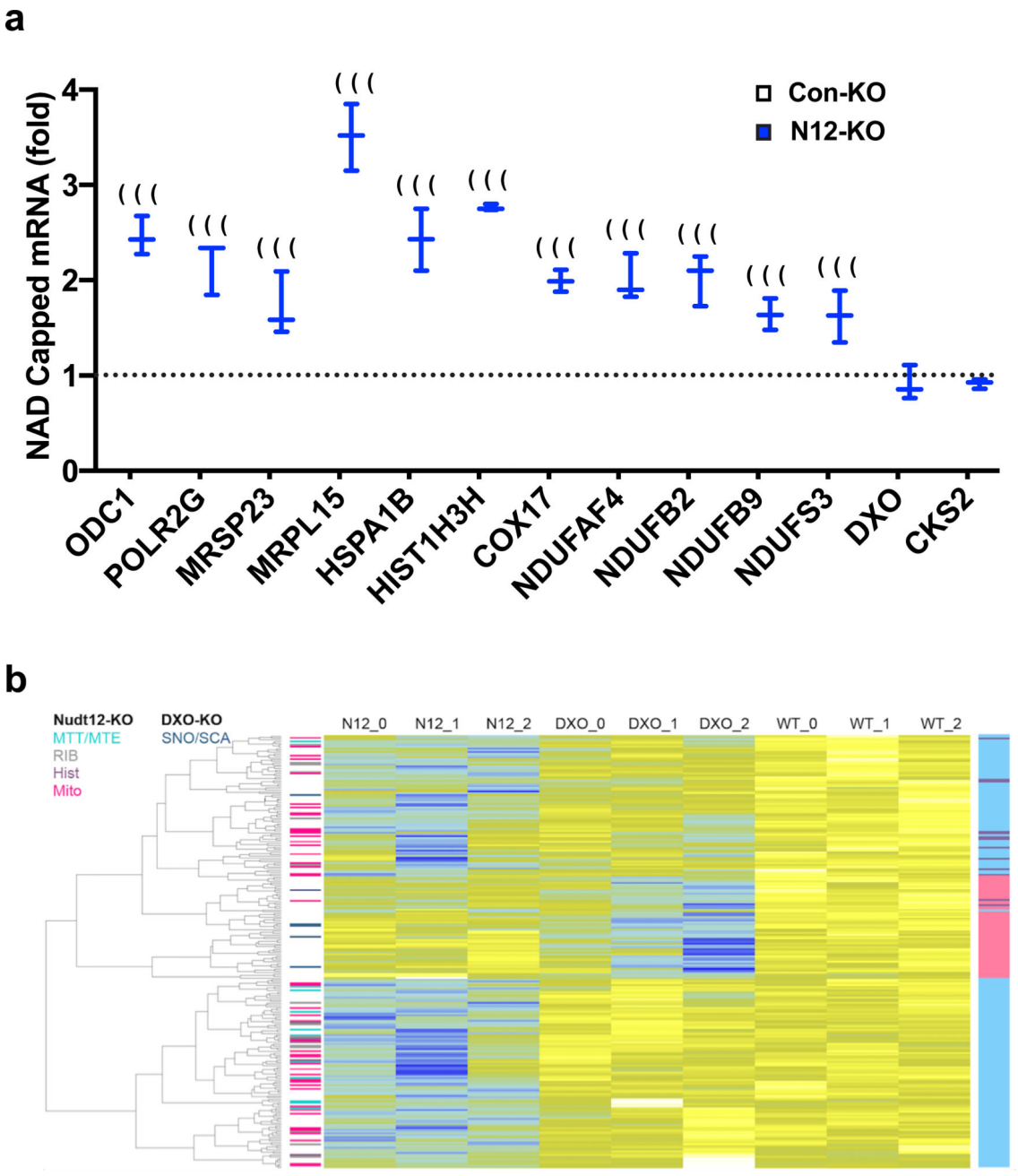

Figure 5. Nudt12 preferentially targets a subset of mRNAs for deNADding

(a) qRT-PCR validation of NAD-capped mRNAs in N12-KO cells. Randomly selected NAD-capped RNAs from the NAD-captureSeq were eluted from the beads, reverse transcribed, and detected with gene-specific primers. Data are presented relative to the HEK293T Con-KO cells set to 1. CKS2, which is not responsive to Nudt12 in the NAD-captureSeq, was included as a negative control (n=3 independent NAD-capture experiments; mean ± SEM; unpaired t test; $p < 0.001$(***)).

(b) Heatmap of mRNAs enriched in either N12-KO or DXO-KO. The color bar at left indicates enriched gene groups, either from top GO biological processes (Supplementary Fig. 5a) or presence of major gene families as indicated (Hist: histones, SNO/SCA:

snoRNAs or scaRNAs). The color bar at right indicates membership in components of Venn diagram (Supplementary Fig. 5b). For each mRNA in the heatmap, blue indicates relative enrichment, yellow indicates relative depletion, with expression normalized for each mRNA across all samples to indicate relative differences. Individual replicate samples from each group are indicated by a trailing number ("_0", "_1", etc.).

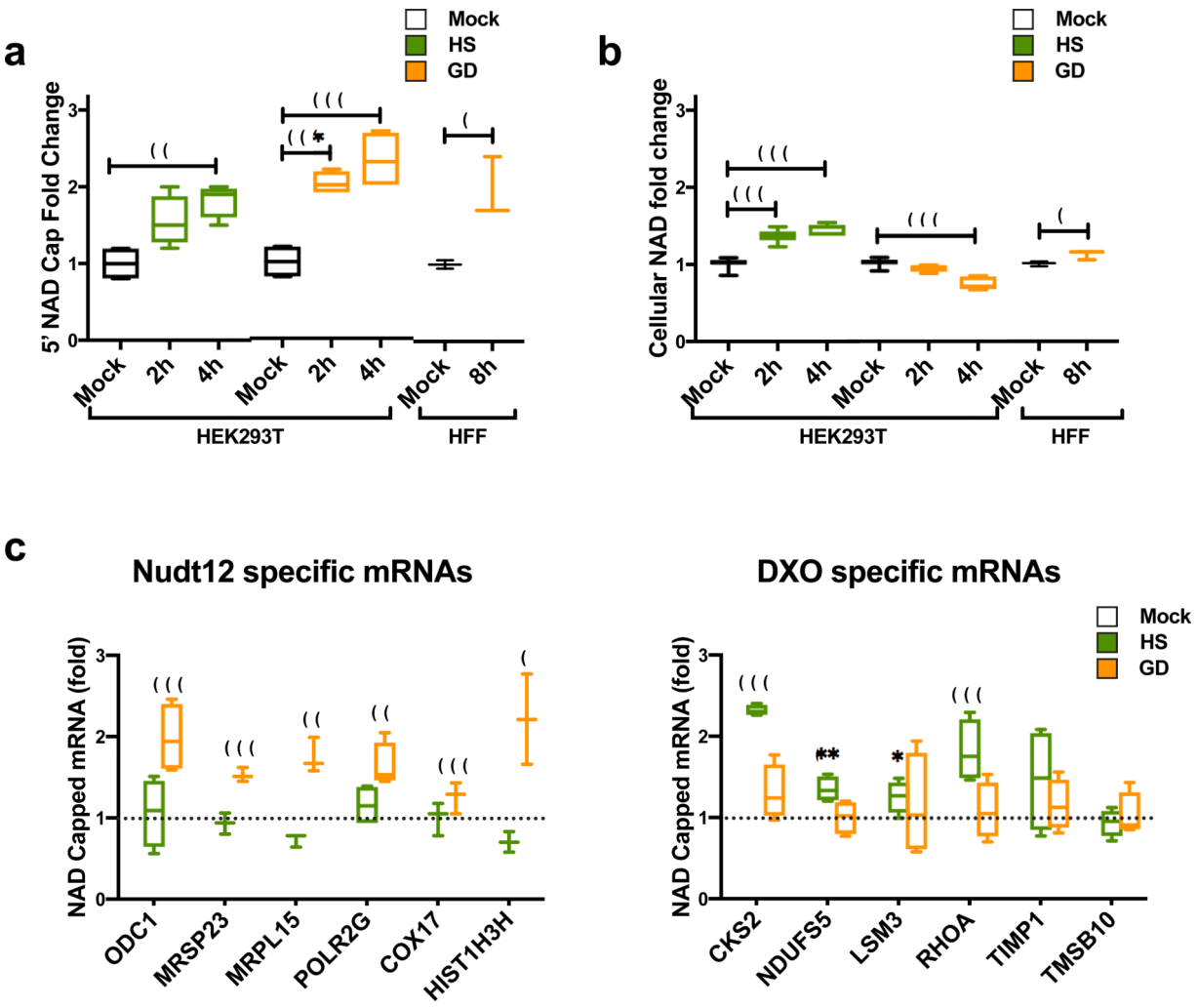

Figure 6. Cellular exposure to stress impacts NAD capping

(a) NAD-capped RNA levels were measured by NAD-capQ in the indicated cells exposed to 42 °C heat shock (HS) or glucose deprivation (GD) for the denoted times. Interleaved box and whiskers show the fold-change in NAD-capped RNA values relative to the value observed in cells that were not subjected to stress. n≥3 independent experiments; mean ± SEM. Data sets for HEK293T cells were analyzed by one-way ANOVA (HS, F=10.23 df=7.651; p=0.0069; GD, F=24.62, df=9, p= 0.0002) with a Dunnett's multiple comparison post hoc test ($p < 0.05$(*), $p < 0.01$(**), $p < 0.001$(***)). Data sets for HFF were analyzed by unpaired t test, t=3.963, df=4, p = 0.0166 (*).

(b) Total cellular NAD levels were detected by colorimetric NAD^+/NADH quantitation assay within the same cells shown in (a). n≥3 independent experiments; mean ± SEM. Data sets for HEK293T cells were analyzed by one-way ANOVA (HS, F=82.39 df=17.8; p<0.0001; GD F=1.254, df=17, p= 0.3105) with a Dunnett's multiple comparison post hoc test ($p < 0.05$(*), $p < 0.01$(**), $p < 0.001$(***)). Data sets for HFF were analyzed by unpaired t test, t=3.028, df=4, p = 0.0389 (*).

(c) QRT-PCR analysis of a subset of Nudt12 or DXO specific NAD-capped mRNAs from HEK293T cells exposed to either 4 hours GD or HS. NAD-capped RNAs isolated by the

NAD-capture approach were eluted from the beads, reverse transcribed, and indicated mRNAs detected with gene-specific primers. Data are presented relative to cells that were not subjected to stress conditions set as 1. (n=3 independent NAD-capture experiments; mean ± SEM; unpaired t test; *, $p < 0.05$; **, $p < 0.01$, ***, $p < 0.001$).